IEEE Access
Multidisciplinary | Rapid Review | Open Access Journal

Received 7 February 2023, accepted 28 February 2023, date of publication 6 March 2023, date of current version 9 March 2023.

Digital Object Identifier 10.1109/ACCESS.2023.3252568

RESEARCH ARTICLE

Binary Radio Tomographic Imaging in Factory Environments Based on LOS/NLOS Identification

TAKAHIRO MATSUDA[1], (Member, IEEE), YOSHIAKI NISHIKAWA[1,2], EIJI TAKAHASHI[2], TAKEO ONISHI[2], AND TOSHIKI TAKEUCHI[3], (Member, IEEE)

[1]Graduate School of Systems Design, Tokyo Metropolitan University, Tokyo 191-0065, Japan
[2]Secure Systems Platforms Research Laboratories, NEC Corporation, Kawasaki, Kanagawa 211-8666, Japan
[3]Advanced Network Research Laboratories, NEC Corporation, Kawasaki, Kanagawa 211-8666, Japan

Corresponding author: Takahiro Matsuda (takahiro.m@tmu.ac.jp)

ABSTRACT *Radio tomographic imaging* (RTI) is a technique for estimating *spatial loss fields* (SLFs), which maps the quantified attenuation of radio signals at every spatial location within monitored regions. In this study, we investigate RTI techniques in indoor factory environments, where the RTI techniques deteriorate because of severe multipath channels. We propose the *binary radio tomographic imaging* (binary RTI) method, where the attenuation level of each pixel in a SLF is defined as a binary value. The binary RTI method is suited for factory environments, including metallic objects, because radio signals are almost fully reflected rather than getting absorbed by such objects. In the proposed method, we suppose that transmitted signals are modulated with an orthogonal frequency division multiplexing (OFDM) format, and each receiver is equipped with multiple antenna elements. By adopting the two-dimensional multiple signal classification (MUSIC), the proposed method identifies whether the signals are transmitted in a line-of-sight (LOS) or a non-line-of-sight (NLOS) path. From the LOS/NLOS identification, we propose two algorithms to estimate the binary SLF: a simple greedy algorithm and a relaxation algorithm with low-rank approximation. We evaluate the performance of the proposed method via simulation experiments. To assess the applicability of the proposed method to factory environments, we assume a severe multipath environment where all the objects, wall, and ceiling are perfect electrical conductors, and show that by using an appropriate threshold parameter for the LOS/NLOS identification, the proposed method can estimate the binary SLF in the test environment.

INDEX TERMS Factory environment, LOS/NLOS identification, radio tomographic imaging.

I. INTRODUCTION

Reliable wireless communication technologies are mandatory for future smart factories [1], [2], [3], [4], and latest wireless network technologies, such as the fifth-generation (5G) cellular network technology for supporting ultra-reliable low-latency communication (URLLC), have garnered significant attention. In this study, we consider industrial Internet of things (IoT) environments based on intelligent vehicles, such as automated guided vehicles (AGVs) and autonomous mobile robots (AMRs) [5], and these vehicles are managed remotely via access points (APs) placed in factory environments. Indoor environments such as office and living spaces are usually open space, primarily because they are designed for comfort. In contrast, factory environments are crowded with objects, such as industrial equipment. Therefore, wireless networks in indoor factory environments must be designed based on different design methodologies.

In [6], an offline method was considered for the faculty radio design using 3D laser scanning and physical optics. In this method, the spatial data of a factory environment, such as the positions and shapes of walls, ceiling, floor, and other objects are first captured by 3D laser scanning. From the scan data, the radio wave propagation is then predicted using physical optics. It is an effective approach in static factory environments in which physical objects and

The associate editor coordinating the review of this manuscript and approving it for publication was Abderrezak Rachedi.

communication devices, such as APs are fixed; however, it is not suitable for non-static environments where their positions are altered, because 3D layer scanning should be conducted each time the positions are changed. To efficiently generate industrial products, facility layouts in factory environments are occasionally reconfigured and optimized, which is referred to as the *factory layout planning problem* [7], [8]. Furthermore, 3D laser scanning is based on physical optics and does not necessarily reflect the characteristics of the radio frequency (RF) signals used for communication, such as diffraction and reflection. Therefore, in this study, we address the factory radio design with RF signals.

We consider *radio tomographic imaging* (RTI) [9], [11], [12], [14], [16], [17], [18], [19], [20], [21] in non-static environments. RTI is a technique for estimating *spatial loss fields* (SLFs), maps quantifying the attenuation of radio signals at each spatial location within monitored regions, and provides useful information for designing reliable wireless networks considering obstructions. In RTI, the monitored region is divided into pixels, and an SLF is represented with a set of attenuation levels of the pixels. The relationship between a measurement vector and an SLF is formulated as a system of linear equations according to the positions of the transmitters and receivers. As it does not require any spatial information of the layout, it is suitable for non-static environments. The formulation is based on an assumption that the received power of a radio signal is dominated by the direct path component in multipath components. However, in factory environments, this assumption is inappropriate because there are several highly reflective metallic objects in the factory environments, which cause severe multipath channels [4], [22].

In this study, we propose *binary radio tomographic imaging* (binary RTI) for factory environments. In factory environments with metallic objects, radio signals are almost fully reflected rather than absorbed. Therefore, we model the attenuation level of each pixel in an SLF with a binary value, i.e., the pixel represents a perfectly reflective object if the attenuation level equals to one, and it does not cause any attenuation if the level is zero.

The proposed method comprises two steps: *line-of-sight (LOS)/non-line-of-sight (NLOS) identification* and *SLF estimation*. In the first step, a transmitted signal between an AP and a mobile terminal is identified as a LOS signal or NLOS signal via of multiple signal classification (MUSIC) [23]. We suppose that transmitted signals are modulated with an orthogonal frequency division multiplexing (OFDM) format and each receiver is equipped with multiple antenna elements. By analyzing an OFDM signal, a 2D MUSIC spectrum is developed as a function angle-of arrivals (AoAs) and time-of arrivals (ToAs) of multipath components (incident signals) in the OFDM signal. From the MUSIC spectrum, the path of each incident signal is identified as LOS or NLOS. In the second step, the SLF is estimated from the results of the first step. The SLF estimation is formulated as a combinatorial optimization problem. First, we consider a greedy algorithm to solve the problem. Furthermore, by relaxing the problem, we consider a low rank approximation to estimate the SLF.

The influence of multipath fading is a well-known problem in RTI and several techniques have been proposed [10], [11], [15], [18], [19], [20] to address these problems. These techniques are classified into (1) the extraction of the direct path component using inverse Fourier transform [11], (2) directional antennas and spatial diversity based on multiple antennas [10], [18], and (3) Bayesian inference [15], [19], [20]. These techniques are reviewed in Section II. The main contributions of this study are as follows.

1) We propose the idea of the binary RTI, which is a completely different approach from existing methods. The proposed method formulates the RTI problem as a combinatorial optimization problem, whereas the conventional RTI methods formulate it as a linear inverse problem. In the conventional methods, a calibration technique, which sets adequate values to parameters, such as the antenna gains and pathloss exponent, is required to correctly retrieve measurement vectors [16]. In contrast, the proposed method does not require any calibration technique as it relies on the LOS/NLOS identification and positions of transmitters and receivers.
2) To estimate SLFs in the binary RTI, we consider two methods: *the simple greedy method* and *the low rank optimization method*, and evaluate these methods through simulation experiments in an indoor wireless channel assuming a factory environment.

The remainder of this paper is organized as follows. In Section II, we review related studies. In Section III, we describe the system model and problem formulation. We propose binary RTI in Section IV, and evaluate the performance of the proposed method in Section V. Finally, we conclude the paper and provide directions for future studies in Section VI.

II. RELATED WORK

RTI techniques have been studied for *device free localization* [9], [11], [18], [19], [20] and *obstacle mapping* [12], [14], [16], [17], [21]. In device free localization, target positions are identified by the change in the SLF. Let $\boldsymbol{x}(t)$ and $\boldsymbol{y}(t)$ denote an SLF and a measurement vector obtained from RSSs between transmitters and receivers at time t, respectively. For given t_1 and t_2 ($t_2 > t_1$), we define the change of $\Delta_{t_1,t_2}\boldsymbol{x}$ and $\Delta_{1,2}\boldsymbol{y}$ as $\Delta_{1,2}\boldsymbol{x} = \boldsymbol{x}(t_2) - \boldsymbol{x}(t_1)$, $\Delta_{1,2}\boldsymbol{y} = \boldsymbol{y}(t_2) - \boldsymbol{y}(t_1)$, respectively, and the relationship between $\Delta_{1,2}\boldsymbol{x}$ and $\Delta_{1,2}\boldsymbol{y}$ is given by

$$\Delta_{1,2}\boldsymbol{y} = \boldsymbol{A}\Delta_{1,2}\boldsymbol{x} + \boldsymbol{w},$$

where $\boldsymbol{A}$ and $\boldsymbol{w}$ represent a measurement matrix and a noise vector, respectively. Since $\Delta_{1,2}\boldsymbol{x}$ includes only the change of the SLF due to moving targets, the positions of the targets can be identified by estimating $\Delta_{1,2}\boldsymbol{x}$. However, obstacle

mapping attempts to reveal obstacles within a measured regions by estimating an SLF. The problem formulation of obstacle mapping is described in Section III. In this study, we focus on obstacle mapping.

As described in Section I, multipath fading deteriorates the performance of RTI and several mitigation techniques of the multipath fading effect have been studied in literature. Table 1 presents a summary of the related works. As mentioned in Section I, these techniques are classified into four types.

Wang et al. [11] proposed a multipath mitigation technique to extract the direct path component in each received signal, which is referred to as the *LOS component* in Section III-D. In this technique, the direct path component is extracted with the chirp FFT. Each transmitter transmits a chirp signal and the received signal is demodulated with a local chirp signal at the receiver. The magnitude of the direct path component is obtained from the fast Fourier transform (FFT) of the demodulated signal.

In [10] and [18], multipath mitigation techniques using directional antennas or spatial diversity are proposed. Kaltiokallio et al. [10] proposed *directional RTI* (dRTI), which mitigates the influence of multipath fading by using electrically switched directional antennas. In [18], spatial diversity was adopted to mitigate the influence of multipath fading. Each wireless node contains multiple antennas, and multiple links are established between transmitters and receivers. The influence of the multipath fading is reduced by averaging the RSS values on these links.

In [15], [19], and [20], Bayesian learning techniques are employed to mitigate the influence of multipath fading. In these techniques, Bayesian modeling is applied to SLFs or noise variance due to multipath fading. In [19], a sparse Bayesian learning approach with the Laplace prior is utilized to enhance the robustness against multipath fading based on the fact that SLFs in device-free localization are sparse. In [15] and [20], a sparse Bayesian approach based on noise adaptive optimization was applied and the influence of multipath fading was modeled with a mixture of Gaussian distribution.

The binary RTI method proposed in this study uses a new approach where elements of SLFs are defined as binary values, where each pixel in an SLF equals to one if there exists some object on it, and it equals to zero otherwise. To the best of our knowledge, this approach has not been considered so far. By binarizing the SLFs, the SLFs can be estimated with LOS/NLOS identification of measurement paths. In other words, accurate levels of LOS components are not required. In a severe multipath environment, the proposed RTI method estimates a two-dimensional MUSIC spectrum as a function of AoAs and ToAs of incident signals in received signals [24], [25], [26], and each received signal is identified as a LOS or a NLOS signal, where a LOS (NLOS) signal implies that it is transferred over a LOS (NLOS) path. To the best of our knowledge, the approach using the LOS/NLOS identification in RTI techniques has not been studied to date.

TABLE 1. Summary of related works on existing multipath mitigation techniques in RTI.

(1) Extraction of direct path components		[11]
(2) Directional antennas and spatial diversity		[10], [18]
(3) Bayesian learning	SLF modeling	[19]
	Noise variance modeling	[15], [20]

The idea of binarization in network performance metrics has been studied in *binary network tomography* (or Boolean network tomography) [29], [30], [31], [32], [33]. Network tomography is a technique for estimating network internal characteristics such as link loss rates and link delays from observable measurements. In binary network tomography techniques, the relationship between end-to-end measurements and links states is formulated as a *group testing* problem [34], and link failures or congested links in a network can be detected from end-to-end measurements. To the best of our knowledge, the proposed binary RTI method is the first technique that adopts this idea in RTI.

III. RADIO TOMOGRAPHIC IMAGING

A. NOTATION

The superscripts $()^{\mathsf{T}}$ and $()^{\mathsf{H}}$ represent the and conjugate transposes, respectively. $\|\cdot\|_p$ $(p = 1, 2)$ represents the ℓ_p norm and for a vector $\boldsymbol{x} = (x_1\ x_2\ \cdots\ x_N)^{\mathsf{T}} \in \mathbb{C}^{N\times 1}$, $\|\boldsymbol{x}\|_p$ is given by

$$\|\boldsymbol{x}\|_p = \left(\sum_{n=1}^{N} |x_n|^p\right)^{1/p}.$$

For a matrix $\boldsymbol{Z} = [z_{n_1,n_2}]_{1\le n_1\le N_1, 1\le n_2\le N_2} \in \mathbb{C}^{N_1\times N_2}$, $\|\boldsymbol{Z}\|_*$ and $\|\boldsymbol{Z}\|_{\mathrm{F}}$ denote the nuclear norm and Frobenius norm of $\boldsymbol{Z}$, respectively, given by

$$\|\boldsymbol{Z}\|_* = \sum_{i=1}^{\min\{N_1,N_2\}} \xi_i, \quad \|\boldsymbol{Z}\|_{\mathrm{F}} = \sum_{i_1}^{N_1}\sum_{i_2}^{N_2} |z_{i_1,i_2}|^2,$$

where ξ_i $(i = 1, 2, \ldots, \min\{N_1, N_2\})$ denote singular values of $\boldsymbol{Z}$.

B. SYSTEM MODEL

Fig. 1 presents an example of the factory layout, where there are N_{AP} APs and N_{MT} mobile terminals (MTs), such as AGVs and AMRs. Let $\mathcal{A}_3 \in \mathbb{R}^3$ denote the entire area in the factory environment, while $\mathcal{A}_2 \in \mathbb{R}^2$ denote the 2D space obtained by projecting $\mathcal{A}_3$ onto the X-Y plane. Let $\boldsymbol{r}_i^{(\mathrm{AP})} = (r_{i,1}^{(\mathrm{AP})}\ r_{i,2}^{(\mathrm{AP})}\ h_{\mathrm{AP}})^{\mathsf{T}} \in \mathcal{A}_3$ $(i = 1, 2, \ldots, N_{\mathrm{AP}})$ and $\boldsymbol{r}_j^{(\mathrm{MT})} = (r_{j,1}^{(\mathrm{MT})}\ r_{j,2}^{(\mathrm{MT})}\ h_{\mathrm{MT}})^{\mathsf{T}} \in \mathcal{A}_3$ $(j = 1, 2, \ldots, N_{\mathrm{MT}})$ denote the positions of the i-th AP and the j-th MT, respectively, where $(r_{i,1}^{(\mathrm{AP})}\ r_{i,2}^{(\mathrm{AP})})^{\mathsf{T}}, (r_{j,1}^{(\mathrm{MT})}\ r_{j,2}^{(\mathrm{MT})})^{\mathsf{T}} \in \mathcal{A}_2$, and h_{AP} and h_{MT} denote the heights of APs and MTs, respectively. We assume that APs are placed at fixed positions and MTs are moving within a restricted area in $\mathcal{A}_3$. Each AP is equipped with N_{A} antenna elements and each MT is equipped with a single antenna element. We assume that MTs can communicate only

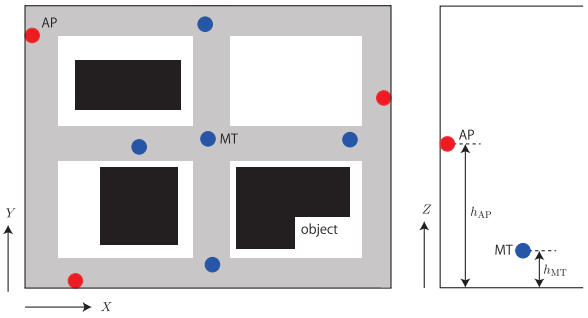

FIGURE 1. System model.

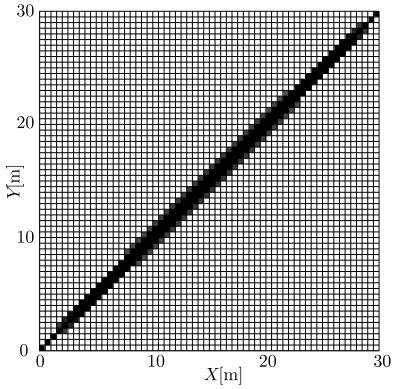

FIGURE 2. Inverse area elliptical model [12], [16] for radio signals with 5 GHz frequency.

with APs and MTs cannot communicate with each other. Moreover, we assume that radio signals are fully reflected by objects in the area.

We define (i_m, j_m) $(m = 1, 2, \ldots, M, i_m = 1, 2, \ldots, N_{\mathrm{AP}}, j_m = 1, 2, \ldots, N_{\mathrm{MT}})$ as the pair of the i_m-th AP and the j_m-th MT, where M denotes the number of pairs. Let P_{i_m,j_m} denote the received power of a radio signal on the (i_m, j_m) link. P_{i_m,j_m} [dBm] is expressed as

$$P_{i_m,j_m} = P_{\mathrm{TX}} - P_{\mathrm{path}}(\|\boldsymbol{r}_{i_m}^{(\mathrm{AP})} - \boldsymbol{r}_{j_m}^{(\mathrm{MT})}\|_2) - S_m - w_m,$$

where P_{TX}, $P_{\mathrm{path}}(\|\boldsymbol{r}_{i_m}^{(\mathrm{AP})} - \boldsymbol{r}_{j_m}^{(\mathrm{MT})}\|_2)$, S_{i_m,j_m}, and w_{i_m,j_m} denote the transmission power, path loss, shadowing loss, and multipath fading loss, respectively. With constant parameters α and β, $P_{\mathrm{path}}(\|\boldsymbol{r}_{i_m}^{(\mathrm{AP})} - \boldsymbol{r}_{j_m}^{(\mathrm{MT})}\|_2)$ is given by

$$P_{\mathrm{path}}(\|\boldsymbol{r}_{i_m}^{(\mathrm{AP})} - \boldsymbol{r}_{j_m}^{(\mathrm{MT})}\|_2) = 10\alpha \log_{10} \|\boldsymbol{r}_{i_m}^{(\mathrm{AP})} - \boldsymbol{r}_{j_m}^{(\mathrm{MT})}\|_2 + \beta,$$

where α $(\alpha \geq 2)$ denotes as the path loss exponent.

C. PROBLEM FORMULATION

If APs and MTs are placed at various heights, SLFs in higher (three or four) dimensional spaces can be estimated using tensor recovery techniques [14]. However, because the heights of APs and MTs are fixed in this study, we focus on the SLF estimation in 2D space $\mathcal{A}_2$.

We divide $\mathcal{A}_2$ into N pixels with the same size. Let x_n $(n = 1, 2, \ldots, N)$ denote the attenuation of signals at pixel n. SLF is then defined as $\boldsymbol{x} = (x_1\ x_2\ \cdots\ x_N)^{\mathsf{T}}$. Assume that P_{TX}, positions $\boldsymbol{r}_{i_m}^{(\mathrm{AP})}$ and $\boldsymbol{r}_{j_m}^{(\mathrm{MT})}$, and parameters α and β are known beforehand. The measurement y_m for (i_m, j_m) is then given by

$$\begin{aligned} y_m &= S_m + w_m \\ &= P_{\mathrm{TX}} - P_{i_m,j_m} - P_{\mathrm{path}}(\|\boldsymbol{r}_{i_m}^{(\mathrm{AP})} - \boldsymbol{r}_{j_m}^{(\mathrm{MT})}\|_2) \end{aligned}$$

S_m can be approximated as a weighted sum of x_n [9] and is described as

$$\begin{aligned} S_m &= \sum_{n=1}^{N} a\left(\boldsymbol{r}_{i_m}^{(\mathrm{AP})}, \boldsymbol{r}_{j_m}^{(\mathrm{MT})} \middle| \tilde{\boldsymbol{r}}_n\right) x_n = \sum_{n=1} a_{m,n} x_n \\ a_{m,n} &\triangleq a\left(\boldsymbol{r}_{i_m}^{(\mathrm{AP})}, \boldsymbol{r}_{j_m}^{(\mathrm{MT})} \middle| \tilde{\boldsymbol{r}}_n\right) \end{aligned}$$

where $\tilde{\boldsymbol{r}}_n$ denotes the center position of pixel n. We define the measurement vector $\boldsymbol{y} = (y_1\ y_2\ \cdots\ y_M)^{\mathsf{T}}$. The relationship between $\boldsymbol{y}$ and $\boldsymbol{x}$ is described as

$$\boldsymbol{y} = \boldsymbol{A}\boldsymbol{x} + \boldsymbol{w},$$

where $\boldsymbol{A} = [a_{m,n}]_{1 \leq m \leq M, 1 \leq n \leq N}$ and $\boldsymbol{w} = (w_1\ w_2\ \cdots\ w_M)^{\mathsf{T}}$.

Several models for $a_{m,n}$ have been considered [12]. In the *inverse area elliptical* model [12], [16], $a_{m,n}$ is set to $a_{m,n} = 0$ if $\|\tilde{\boldsymbol{r}}_n - \boldsymbol{r}_{i_m}^{(\mathrm{AP})}\|_2 + \|\tilde{\boldsymbol{r}}_n - \boldsymbol{r}_{j_m}^{(\mathrm{MT})}\|_2 > d + \lambda/2$, where $d = \|\boldsymbol{r}_{i_m}^{(\mathrm{AP})} - \boldsymbol{r}_{j_m}^{(\mathrm{MT})}\|$ and λ denote the wavelength of the radio signals. Otherwise, $a_{m,n}$ is set to

$$a_{m,n} = \frac{4}{\pi \zeta_\beta\left(\tilde{\boldsymbol{r}}_n; \boldsymbol{r}_{i_m}^{(\mathrm{AP})}, \boldsymbol{r}_{j_m}^{(\mathrm{MT})}\right) \sqrt{d^2 + \zeta_\beta^2\left(\tilde{\boldsymbol{r}}_n; \boldsymbol{r}_{i_m}^{(\mathrm{AP})}, \boldsymbol{r}_{j_m}^{(\mathrm{MT})}\right)}},$$

$$\begin{aligned} &\zeta_\beta\left(\boldsymbol{r}_n; \boldsymbol{r}_{1,i_m}, \boldsymbol{r}_{2,j_m}\right) \\ &= \sqrt{\max\left\{\beta^2, \left(\|\boldsymbol{r}_n - \boldsymbol{r}_{1,i_m}\|_2 + \|\boldsymbol{r}_n - \boldsymbol{r}_{2,j_m}\|_2\right)^2 - d^2\right\}}. \end{aligned}$$

Fig. 2 presents examples of weights when the inverse area elliptical model is used.

D. INFLUENCE OF MULTIPATH FADING

In a multipath channel, the channel impulse response $h(\tau)$ can be described as

$$h(\tau) = \sum_{l=1}^{L} h_l \delta(\tau - \tau_l), \tag{1}$$

where L, h_l, and τ_l denote the number of paths, complex amplitude of the l-th path, and delay of the l-th path, respectively. Without loss of generality, we set $\tau_1 < \tau_2 < \cdots < \tau_L$. The first path then corresponds to the direct path. Let P_{TX} denote the transmission power of radio signals. The received power P_{RX} of a radio signal and the power P_{LOS} of the direct path are given by

$$P_{\mathrm{RX}} = P_{\mathrm{TX}} \sum_{l=1}^{L} |h_l|^2, \quad P_{\mathrm{LOS}} = P_{\mathrm{TX}} |h_1|^2,$$

respectively. We refer to P_{LOS} as the *LOS component* of the channel. To represent LOS and NLOS signals in a

unified manner, we consider that NLOS signals have the LOS component with $h_1 = 0$.

Fig. 3 presents the received powers of radio signals measured in the simulation environment in Section V. Figs. 3a and 3b exhibit received powers of LOS signals and NLOS signals vs. the distance between transmitters and receivers, respectively. We observe that NLOS signals have comparable received powers even though they have no direct path component. As demonstrated by the inverse area elliptical model in Section III-C, each element in measurement vector $\boldsymbol{y}$ is dominated by the LOS component. Therefore, these figures indicate that the SLF is underestimated, particularly in pixels that these NLOS signals pass through. Fig. 3c presents LOS components vs. received powers for LOS signals. We observe that some signals have significantly smaller received powers although the direct path components are included in the signals. These LOS signals trigger the overestimation of the SLF in some pixels because RTI considers that the signals are highly attenuated.

In summary, highly reflective areas such as factory environments deteriorate the performance of RTI. In the proposed method, we address this problem by LOS/NLOS identification.

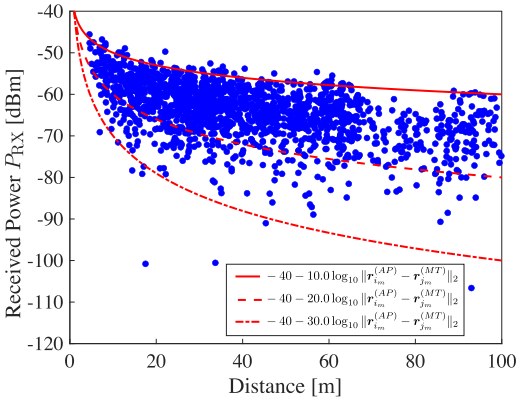

(a) Received powers of LOS signals vs. distance.

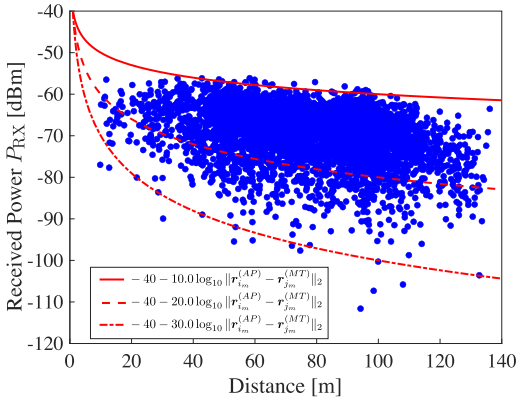

(b) Received powers of NLOS signals vs. distance.

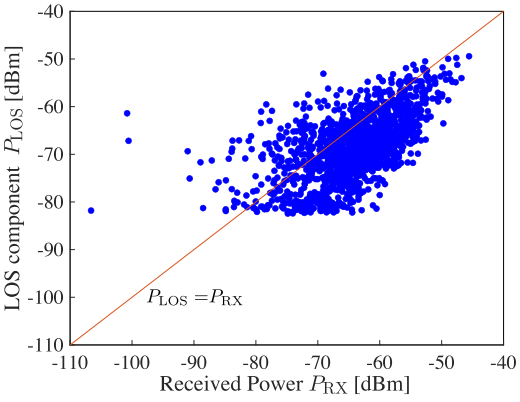

(c) LOS components vs. received powers.

FIGURE 3. Received powers of LOS and NLOS signals.

IV. BINARY RADIO TOMOGRAPHIC IMAGING BASED ON LOS/NLOS IDENTIFICATION

Fig. 4 presents the overview of the proposed binary RTI. Let $\boldsymbol{Y}^{(m)} = [y_{n_{\mathrm{A}},k}^{(m)}]_{1\le n_{\mathrm{A}}\le N_{\mathrm{A}},1\le k\le N_{\mathrm{SC}}} \in \mathbb{C}^{n_{\mathrm{A}}\times N_{\mathrm{SC}}}$ denote the OFDM signal transmitted from the j_m-th MT and received at the i_m-th AP, where N_{SC} represents the number of subcarriers of the OFDM signal. *Path state* q_m $(m = 1, 2, \ldots, M)$ represents the type of the (i_m, j_m)-th path, where $q_m = 0$ if the path is LOS and $q_m = 1$ otherwise. From $\boldsymbol{Y}^{(i_m,j_m)}$, q_m is estimated via the two-dimensional MUSIC method, which is described by Section IV-A.

In the binary RTI, SLF $\boldsymbol{x} = (x_1\ x_2\ \cdots\ x_N)^{\mathsf{T}}$ is defined as a vector with binary elements, where $x_n = 1$ if there is an object to attenuate the signal power in the pixel n, and $x_n = 0$ otherwise. $\boldsymbol{x}$ is estimated from the estimated path states $\hat{\boldsymbol{q}} = (\hat{q}_1\ \hat{q}_2\ \cdots\ \hat{q}_M)^{\mathsf{T}}$. The algorithms to estimate $\boldsymbol{x}$ are described in section IV-B. We assume that SLF $\boldsymbol{x}$ does not change when estimating it. Therefore, $\boldsymbol{x}$ is estimated after all q_m $(m = 1, 2, \ldots, M)$ are obtained. Sequential or adaptive estimators of $\boldsymbol{x}$ are not considered in this study.

A. LOS/NLOS IDENTIFICATION

Let $h_{n_{\mathrm{A}}}(t)$ denote the channel impulse response of signals received at the n_{A}-th antenna element $(n_{\mathrm{A}} = 1, 2, \ldots, N_{\mathrm{A}})$. From (1), $h_{n_{\mathrm{A}}}(\tau)$ can be expressed as

$$h_{n_{\mathrm{A}}}(\tau) = \sum_{l=1}^{L} c_l a_{n_{\mathrm{A}}}(\theta_l)\delta(\tau - \tau_l),$$

where c_l θ_l denote the complex channel gain and AoA of the l-th path, respectively. When adopting a uniform linear array with n_{A} antenna elements spaced by d, $a_{n_{\mathrm{A}}}(\theta)$ is given by

$$a_{n_{\mathrm{A}}}(\theta_l) = \exp\left(-j\frac{2\pi(n_{\mathrm{A}}-1)d\sin(\theta_l)}{\lambda}\right),$$

where λ denotes the carrier wavelength. Let $f_k = (k-1)f_0$ denote the k-th subcarrier frequency, where f_0 represents the subcarrier spacing. Subsequently, the t-th received coefficient $y_{n_{\mathrm{A}},k}^{(m)}(t)$ $(t = 1, 2, \ldots, T)$ of the k-th subcarrier at the n_{A}-th antenna element is then given by

$$y_{n_{\mathrm{A}},k}^{(m)}(t) = \sum_{l=1}^{L} s_k^{(m)}(t)c_l^{(m)}(t)a_{n_{\mathrm{A}}}(\theta_l)\exp(-j2\pi f_k\tau_l) + \eta_{n_{\mathrm{A}},k}^{(m)}(t),$$

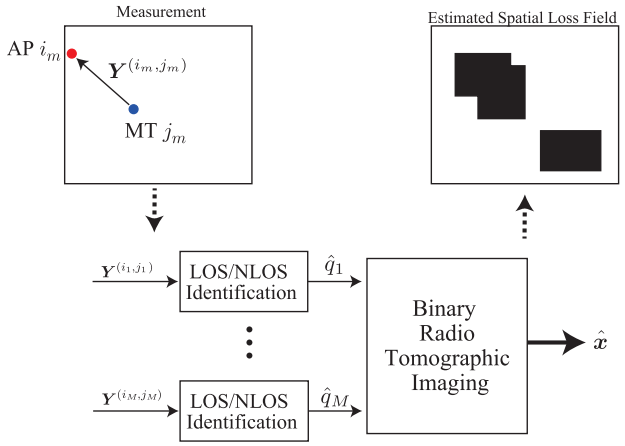

FIGURE 4. Overview of binary RTI.

where $\eta^{(m)}_{n_\mathrm{A},k}(t)$ and T denote the noise and number of received signals, respectively. $s^{(m)}_k(t)$ ($|s^{(m)}_k(t)| = 1, k = 1, 2, \ldots, K$) are transmitted symbols at sub-carrier f_k and we define $\boldsymbol{y}^{(m)}(t) = (y^{(m)}_{1,1}(t)\ y^{(m)}_{1,2}(t)\ \cdots\ y^{(m)}_{N_\mathrm{A},K}(t))^\mathsf{T}$. In this subsection, we focus on the LOS/NLOS identification for the (i_m, j_m)-th path, and omit the superscript (m) to simplify the notation.

We define steering vector $\boldsymbol{b}(\theta_l, \tau_l)$ as

$$\begin{aligned}\boldsymbol{b}(\theta_l, \tau_l) &= (b_{1,1}(\theta_l, \tau_l)\ b_{1,2}(\theta_l, \tau_l)\ \cdots\ b_{N_\mathrm{A},K}(\theta_l, \tau_l))^\mathsf{T}\\ b_{n_\mathrm{A},k}(\theta_l, \tau_l) &= a_{n_\mathrm{A}}(\theta_l)\exp(-j2\pi f_k \tau_l),\\ &= \exp\left(-j\frac{2\pi(n_\mathrm{A}-1)d\sin(\theta_l)}{\lambda}\right)\\ &\quad\cdot\exp(-j2\pi f_k\tau_l).\end{aligned}$$

$\boldsymbol{y}(t)$ is then expressed as

$$\begin{aligned}\boldsymbol{y}(t) &= \boldsymbol{S}(t)\,(\boldsymbol{b}(\theta_1,\tau_1)\,\boldsymbol{b}(\theta_2,\tau_2)\ \cdots\ \boldsymbol{b}(\theta_L,\tau_L))\,\boldsymbol{c}(t) + \boldsymbol{\eta}(t)\\ &= \boldsymbol{S}(t)\boldsymbol{B}\boldsymbol{c}(t) + \boldsymbol{\eta}(t),\\ \boldsymbol{S}(t) &= \mathrm{diag}(\boldsymbol{s}(t)\ \boldsymbol{s}(t)\ \cdots\ \boldsymbol{s}(t))\\ \boldsymbol{s}(t) &= (s_1(t)\ s_2(t)\ \cdots\ s_K(t))\\ \boldsymbol{B} &= (\boldsymbol{b}(\theta_1,\tau_1)\,\boldsymbol{b}(\theta_2,\tau_2)\ \cdots\ \boldsymbol{b}(\theta_L,\tau_L))\,,\\ \boldsymbol{c}(t) &= (c_1(t)\ c_2(t)\ \cdots\ c_L(t))^\mathsf{T}\\ \boldsymbol{\eta}(t) &= (\eta_{1,1}(t)\ \eta_{1,2}(t)\ \cdots\ \eta_{N_\mathrm{A},K}(t))^\mathsf{T}.\end{aligned}$$

Since $\boldsymbol{S}(t)$ represents a diagonal matrix and $|s_k(t)| = 1$, we obtain

$$\boldsymbol{S}(t)\boldsymbol{B}\boldsymbol{c}(t)\boldsymbol{c}^\mathsf{H}(t)\boldsymbol{B}^\mathsf{H}\boldsymbol{S}^\mathsf{H}(t) = \boldsymbol{B}\boldsymbol{c}(t)\boldsymbol{c}^\mathsf{H}(t)\boldsymbol{B}^\mathsf{H}.$$

By assuming that $\eta_{n_\mathrm{A},k}(t)$ ($n_\mathrm{A} = 1, 2, \ldots, N_\mathrm{A}, k = 1, 2, \ldots, K$) are zero mean uncorrelated complex Gaussian variables with variance σ^2_η, the correlation matrix $\boldsymbol{R}$ is obtained as

$$\begin{aligned}\boldsymbol{R} &= \mathbb{E}(\boldsymbol{y}(t)\boldsymbol{y}^\mathsf{H}(t))\\ &= \boldsymbol{B}\mathbb{E}(\boldsymbol{c}(t)\boldsymbol{c}^\mathsf{H}(t))\boldsymbol{B}^\mathsf{H} + \sigma^2_\eta\boldsymbol{I}_{N_\mathrm{A}K},\end{aligned}$$

where $\boldsymbol{I}_{N_\mathrm{A}K}$ denotes the $N_\mathrm{A}K \times N_\mathrm{A}K$ identity matrix.

Let μ_p and $\boldsymbol{u}_p$ ($p = 1, 2, \ldots, N_\mathrm{A}K$, $\mu_1 \geq \mu_2 \geq \cdots \mu_{N_\mathrm{A}K}$) denote the p-th eigenvalue of $\boldsymbol{R}$ and the eigenvector associated with μ_p. We define a column span $\mathcal{S} = \mathrm{span}\{\boldsymbol{u}_1, \boldsymbol{u}_2, \ldots, \boldsymbol{u}_{N_\mathrm{A}K}\}$ and divide $\mathcal{S}$ into a *signal subspace* $\mathcal{S}_\mathrm{S} = \mathrm{span}\{\boldsymbol{u}_1, \boldsymbol{u}_2, \ldots, \boldsymbol{u}_{N_\mathrm{S}}\}$ and a *noise subspace* $\mathcal{S}_\mathrm{N} = \mathrm{span}\{\boldsymbol{e}_1, \boldsymbol{e}_2, \ldots, \boldsymbol{e}_{N_\mathrm{N}}\}$, where $N_\mathrm{S} + N_\mathrm{N} = MK$ and $\boldsymbol{e}_p = \boldsymbol{u}_{p+N_\mathrm{S}}$ ($p = 1, 2, \ldots, N_\mathrm{N}$). The MUSIC spectrum $P_\mathrm{MUSIC}(\theta, \tau)$ is then defined as

$$P_\mathrm{MUSIC}(\theta,\tau) = \frac{\boldsymbol{b}^\mathsf{H}(\theta,\tau)\boldsymbol{b}(\theta,\tau)}{\boldsymbol{b}^\mathsf{H}(\theta,\tau)\boldsymbol{E}_\mathrm{N}\boldsymbol{E}_\mathrm{N}^\mathsf{H}\boldsymbol{b}(\theta,\tau)},$$

where $\boldsymbol{E}_\mathrm{N} = (\boldsymbol{e}_1\ \boldsymbol{e}_2\ \cdots\ \boldsymbol{e}_{N_\mathrm{N}})$. We assume that all the MTs are perfectly localized by adopting a localization method without RF signals such as light detection and ranging (LiDAR) [36], [37], [38]. Recall that $\boldsymbol{r}^{(\mathrm{AP})}_{i_m}$ and $\boldsymbol{r}^{(\mathrm{MT})}_{j_m}$ represent the positions of AP i_m and MT j_m ($m = 1, 2, \ldots, M$), respectively. We define $\hat{\theta}_\mathrm{LOS}(i_m, j_m)$ as the direction of the direct path on (i_m, j_m), which can be computed from $\boldsymbol{r}^{(\mathrm{AP})}_{i_m} - \boldsymbol{r}^{(\mathrm{MT})}_{j_m}$, and $\hat{\tau}_\mathrm{LOS}(i_m, j_m)$ as

$$\hat{\tau}_\mathrm{LOS}(i_m,j_m) = \frac{\|\boldsymbol{r}^{(\mathrm{AP})}_{i_m} - \boldsymbol{r}^{(\mathrm{MT})}_{j_m}\|_2}{c},$$

where c denotes the speed of light.

With threshold P_th, q_m is given by

$$q_m = \begin{cases}0 & \text{if } P_\mathrm{MUSIC}(\hat{\theta}_\mathrm{LOS}(i_m,j_m),\ \hat{\tau}_\mathrm{LOS}(i_m,j_m)) \geq P_\mathrm{th}\\ 1 & \text{otherwise}\end{cases}$$

Since $\boldsymbol{E}_\mathrm{N}\boldsymbol{E}_\mathrm{N}^\mathsf{H}$ has N_N eigenvalues of 1,

$$\frac{\boldsymbol{z}^\mathsf{H}\boldsymbol{E}_\mathrm{N}\boldsymbol{E}_\mathrm{N}^\mathsf{H}\boldsymbol{z}}{\boldsymbol{z}^\mathsf{H}\boldsymbol{z}} \leq 1,$$

for arbitrary complex vector $\boldsymbol{z} \in \mathbb{C}^{N_\mathrm{A}K\times 1}$. Therefore, we set $P_\mathrm{th} > 1$.

In general, for AoA estimation problems, to identify AoAs, it is necessary to search peaks in the MUSIC spectrum with a peak search algorithm [39], or to solve a polynomial equation in Root-MUSIC methods [40]. However, in the proposed method, the above LOS/NLOS identification method is advantageous in terms of computational complexity because it does not require such a peak search technique.

B. BINARY RADIO TOMOGRAPHIC IMAGING

We define $\mathcal{Q}_m \subset \{1, 2, \ldots, N\}$, where $n \in \mathcal{Q}_m$ if the line between AP i_m and MT j_m crosses the pixel n. The relationship between $\boldsymbol{x}$ and $\boldsymbol{q}$ can be described as

$$\begin{aligned}q_m &= \bigvee_{n\in\mathcal{Q}(m)} a_{m,n}\wedge x_n\\ &= (a_{m,1}\wedge x_1)\vee(a_{m,2}\wedge x_2)\vee\cdots(a_{m,n}\wedge x_n),\\ a_{m,n} &= \begin{cases}1 & n\in\mathcal{Q}_m\\ 0 & n\notin\mathcal{Q}_m,\end{cases}\end{aligned} \tag{2}$$

where $\vee$ and $\wedge$ represent OR and AND operations, respectively. The binary RTI attempts to estimate $\boldsymbol{x}$ from $\hat{\boldsymbol{q}}$, and from the above relationship, this problem can be formulated as a combinatorial optimization problem. In this study, we consider two methods to solve the binary RTI problem: a *simple method* and *low rank approximation method*.

Algorithm 1 Greedy Algorithm for Binary RTI

Input: y_m, $\mathcal{Q}_m$ $(m = 1, 2, \ldots, M)$
Output: x_n $(n = 1, 2, \ldots, N)$

```
x_n := 1 (n = 1, 2, ..., N)
for m = 1 to M do
    if y_m = 0 then
        for all n ∈ Q_m do
            x_n := 0
        end for
    end if
end for
```

1) SIMPLE METHOD

Algorithm 1 outlines the algorithm of the simple method, which is a type of greedy algorithms. Initially, all elements of $\boldsymbol{x}$ are set to one, which implies that there are objects in all pixels. If the path (i_m, j_m) is identified as LOS (that is, $\hat{q}_m = 0$), x_n for $\forall n \in \mathcal{Q}_m$ are changed to $x_n = 0$. Although this algorithm is very simple, pixels that are not included in any path are estimated to be one.

2) LOW RANK OPTIMIZATION METHOD

The low rank approximation method comprises *optimization*, *filtering*, and *binarization*. In optimization, the SLF is estimated from estimated path states $\hat{\boldsymbol{q}}$. The estimated SLF includes *impulsive noise*, also known as *salt-and-pepper noise* in image processing. Specifically, there is a small number of pixels with values more than zero in areas that most pixels have zero values. The impulsive noise is discarded by filtering. Finally, the filtered SLF is binarized by comparing each pixel with threshold.

a: OPTIMIZATION

In the low rank optimization method, x_n $(n = 1, 2, \ldots, N)$ are relaxed to real values satisfying $0 \le x_n \le 1$. From (2), x_n satisfies the following equations:

$$\sum_{n \in \mathcal{Q}_m} a_{m,n} x_n = 0 \quad \text{if } q_m = 0,$$
$$\sum_{n \in \mathcal{Q}_m} a_{m,n} x_n \ge 1 \quad \text{if } q_m = 1.$$

We assume that $\mathcal{A}_2$ is a rectangular area with $W_1 \times W_2$ [m^2] and it is divided it into $N_1 \times N_2$ pixels with a size of $\delta \times \delta$ [m^2]. We define $\boldsymbol{Z} = [z_{n_1,n_2}]_{1 \le n_1 \le N_1, 1 \le n_2 \le N_2}$ as $z_{n_1,n_2} = x_{n_1+(n_2-1)N_1}$, i.e., $\boldsymbol{Z}$ is a matricization of $\boldsymbol{x}$. We assume that $\boldsymbol{Z}$ is an approximately low rank matrix. For a given $\hat{\boldsymbol{q}}$, $\boldsymbol{Z}$ can be estimated by using a nuclear norm optimization with total variation [41]:

$$\min_{\boldsymbol{Z}} \ (1-\gamma)\|\boldsymbol{Z}\|_* + \gamma \left(\|\boldsymbol{\Phi}\boldsymbol{Z}\|_{\mathrm{F}} + \|\boldsymbol{Z}\boldsymbol{\Psi}\|_{\mathrm{F}}\right)$$
$$\text{subject to} \sum_{n_1+(n_2-1)N_1 \in \mathcal{Q}_m} a_{m,n} z_{n_1,n_2} = 0 \quad \text{if } \hat{q}_m = 0,$$
$$\sum_{n_1+(n_2-1)N_1 \in \mathcal{Q}_m} a_{m,n} z_{n_1,n_2} \ge 1 \quad \text{if } \hat{q}_m = 1,$$

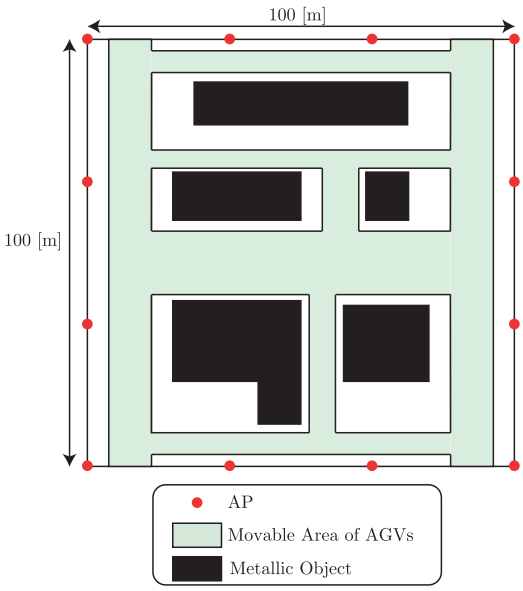

FIGURE 5. Factory environment for simulation experiments.

TABLE 2. Parameters for simulation experiments.

carrier frequency K	5 [GHz]
subcarrier space f_0	312.5 [kHz]
The number of subcarriers N_{SC}	256
transmission power	10 [dBm]
The number of antenna elements n_{A}	$1, 2, 4, 8$
antenna array configuration	uniform linear array
radiation pattern of each antenna element	omni-directional

$$0 \le z_{n_1,n_2} \le 1$$
$$n_1 = 1, 2, \ldots, N_1, \quad n_2 = 1, 2, \ldots, N_2, \qquad (3)$$

where $\boldsymbol{\Phi} = [\phi_{i_1,i_2}]_{1 \le i_1,i_2 \le N_1}$ and $\boldsymbol{\Psi} = [\psi_{j_1,j_2}]_{1 \le j_1,j_2 \le N_2}$ are given by

$$\phi_{i_1,i_2} = \begin{cases} 1 & \text{if } i_1 = i_2, 1 \le i_1, i_2 \le N_1 - 1 \\ -1 & \text{if } i_2 = i_1 + 1, 1 \le i_1 \le N_1 - 1 \\ 0 & \text{otherwise,} \end{cases}$$
$$\psi_{j_1,j_2} = \begin{cases} 1 & \text{if } j_1 = j_2, 1 \le j_1, j_2 \le N_1 - 1 \\ -1 & \text{if } j_2 = j_1 - 1, 2 \le j_1 \le N_1 \\ 0 & \text{otherwise.} \end{cases}$$

b: FILTERING

To discard impulsive noise, we apply a two dimensional *median filter* to the estimated SLF $\boldsymbol{Z}^{(\mathrm{LR})} = [z^{(\mathrm{LR})}_{n_1,n_2}]_{1 \le n_1 \le N_1, 1 \le n_2 \le N_2}$ with the nuclear norm optimization (3). The median filtered SLF $\boldsymbol{Z}^{(\mathrm{Med})} = [z^{(\mathrm{Med})}_{n_1,n_2}]$ is given by [42]

$$z^{(\mathrm{Med})}_{n_1,n_2} = \mathrm{median}\{z^{(\mathrm{LR})}_{n_1-i_1,n_2-i_2} \mid (i_1, i_2) \in \mathcal{W}\},$$

where $\mathcal{W}$ represents a window. In this study, we adopt the (3×3) window. The median filter is a non-linear filter and is beneficial for eliminating impulsive noise.

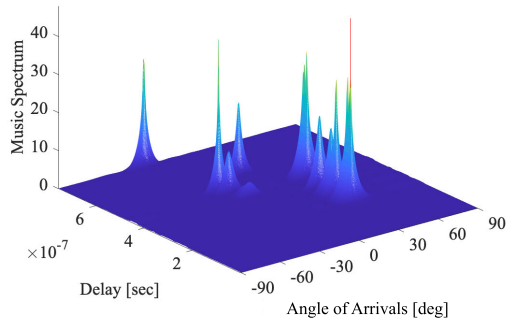

(a) LOS

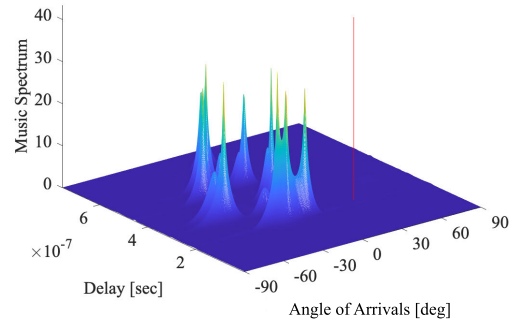

(b) NLOS

FIGURE 6. MUSIC spectrums for LOS and NLOS environments. Red lines correspond to $(\hat{\theta}_{\mathrm{LOS}}(i_m, j_m), \hat{\tau}_{\mathrm{LOS}}(i_m, j_m))$.

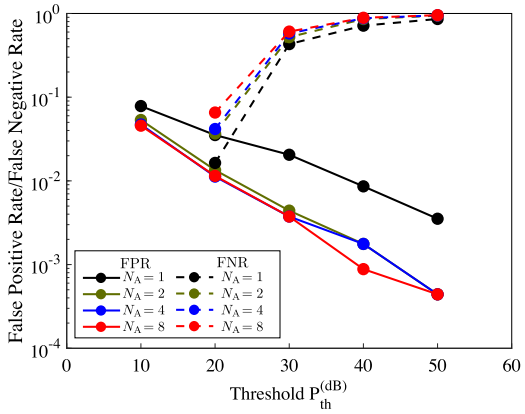

FIGURE 7. FPR and FNR vs. threshold $P_{\mathrm{th}}^{(\mathrm{dB})}$.

c: BINARIZATION

Each element in $\boldsymbol{Z}^{(\mathrm{Med})}$ is binarized by comparing $z_{n_1,n_2}^{(\mathrm{Med})}$ with z_{th}, and finally $\boldsymbol{Z}^{(\mathrm{Bin})} = [z_{n_1,n_2}^{(\mathrm{Bin})}]$ is obtained, i.e.,

$$z_{n_1,n_2}^{(\mathrm{Bin})} = \begin{cases} 1 & z_{n_1,n_2}^{(\mathrm{Med})} \geq z_{\mathrm{th}} \\ 0 & z_{n_1,n_2}^{(\mathrm{Med})} < z_{\mathrm{th}}. \end{cases}$$

To obtain z_{th}, we apply the *Otsu's threshold selection method* [43].

V. PERFORMANCE EVALUATION

A. SIMULATION ENVIRONMENT

In this section, we evaluate the performance of the proposed binary RTI method with simulation experiments. Fig. 5 presents the factory environment for simulation experiments, where $W_1 = W_2 = 100$ [m] and 12 APs were placed at $h_{\mathrm{AP}} = 5$ [m]. We set $\delta = 2.5$ [m]; hence, $N_1 = N_2 = 40$. Bärring et al. [6] adopted a simplified simulation model for factory environments, where only flat and slowly curved surfaces of scatters are supported. Moreover, the materials of the walls, floor, and ceiling are assumed to be perfect electrical conductors (PECs). In this study, we adopt a similar simplified model with simple shaped objects in the rectangular area, and assume that all the objects, walls, and ceiling are PECs, and the floor is concrete. MTs are randomly placed within the movable area in the figure and we set $h_{\mathrm{MT}} = 2.0$ [m]. Radio channels between APs and MTs are generated with EEM-RTM [44], which is a ray-launching-based radio propagation simulator.

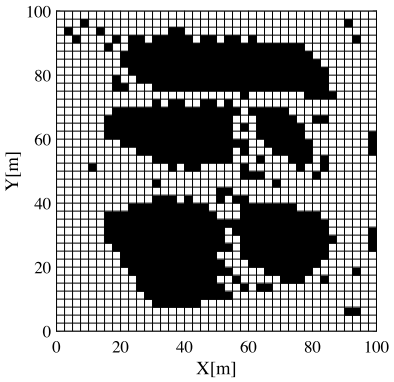

(a) $P_{\mathrm{th}}^{(\mathrm{dB})} = 20$ [dB].

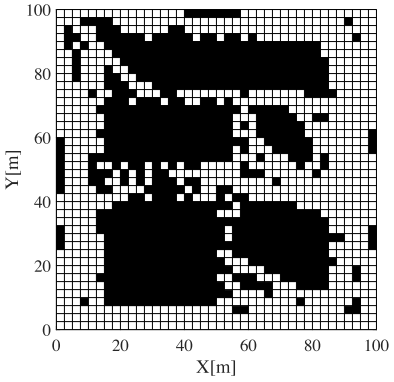

(b) $P_{\mathrm{th}}^{(\mathrm{dB})} = 30$ [dB].

FIGURE 8. Estimated SLF with the simple method.

Note that the localization error affects the performance of the proposed method because $\hat{\theta}_{\mathrm{LOS}}(i_m, j_m)$ and $\hat{\tau}_{\mathrm{LOS}}(i_m, j_m)$ $(m = 1, 2, \ldots, M)$ are computed from position $\boldsymbol{r}_{j_m}^{(\mathrm{MT})}$ of MT j_m, as described in section IV-A. However, in this study, we do not consider the localization error. More specifically, we assume an ideal situation where all MTs are perfectly localized. The reason is that the aim of this study is to demonstrate the basic performance of the binary RTI. In the future research, we will consider a *joint localization and RTI* method, which combines the binary RTI method with a localization algorithm.

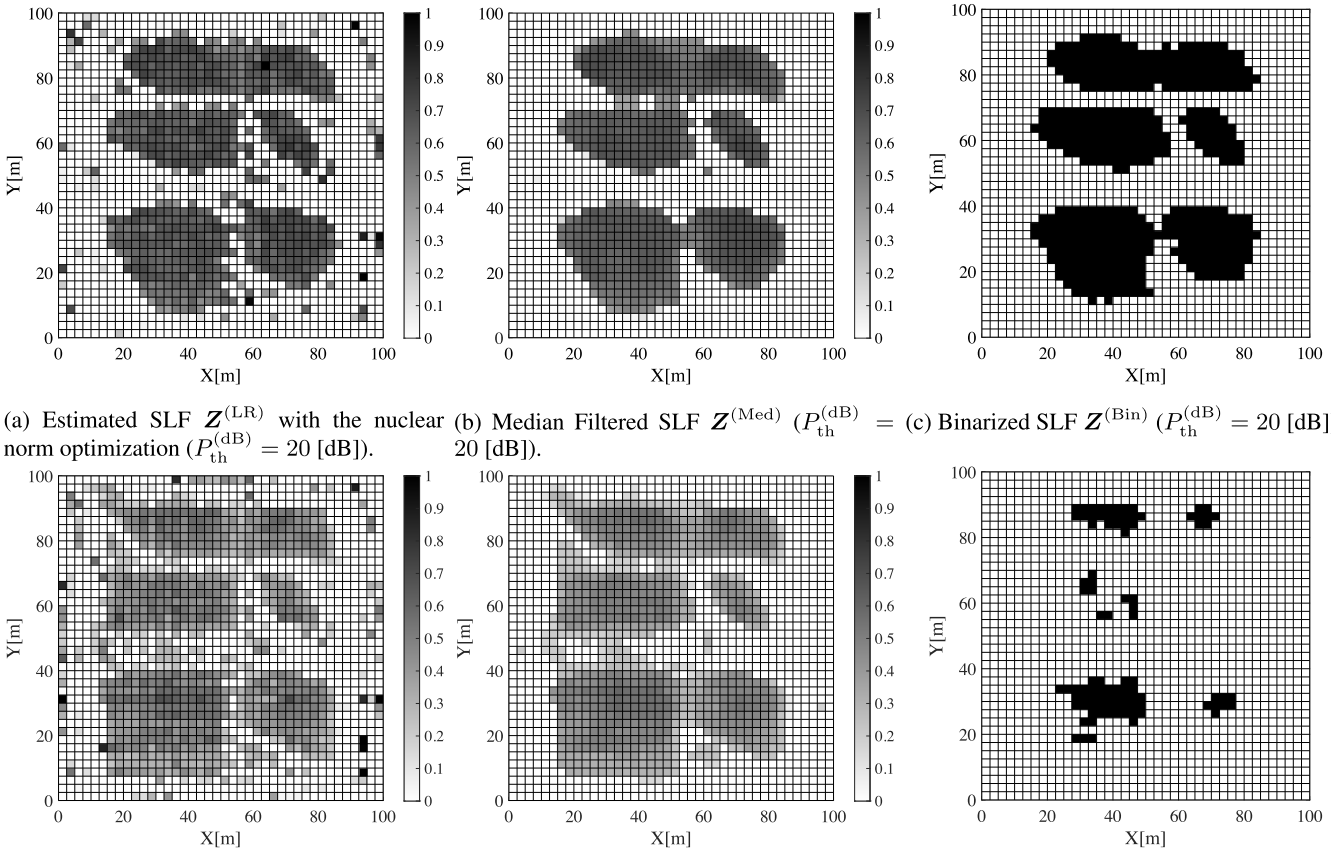

(a) Estimated SLF $\boldsymbol{Z}^{(\mathrm{LR})}$ with the nuclear norm optimization ($P_{\mathrm{th}}^{(\mathrm{dB})} = 20$ [dB]).
(b) Median Filtered SLF $\boldsymbol{Z}^{(\mathrm{Med})}$ ($P_{\mathrm{th}}^{(\mathrm{dB})} = 20$ [dB]).
(c) Binarized SLF $\boldsymbol{Z}^{(\mathrm{Bin})}$ ($P_{\mathrm{th}}^{(\mathrm{dB})} = 20$ [dB]).
(d) Estimated SLF $\boldsymbol{Z}^{(\mathrm{LR})}$ with the nuclear norm optimization ($P_{\mathrm{th}}^{(\mathrm{dB})} = 30$ [dB]).
(e) Median Filtered SLF $\boldsymbol{Z}^{(\mathrm{Med})}$ ($P_{\mathrm{th}}^{(\mathrm{dB})} = 30$ [dB]).
(f) Binarized SLF $\boldsymbol{Z}^{(\mathrm{Bin})}$ ($P_{\mathrm{th}}^{(\mathrm{dB})} = 30$ [dB]).

FIGURE 9. Estimated SLFs with low-rank approximation method for $P_{\mathrm{th}}^{(\mathrm{dB})} = 20$ [dB] (upper) and $P_{\mathrm{th}}^{(\mathrm{dB})} = 30$ [dB] (lower).

Table 2 presents the parameters for radio signals. For each received signal, we added a noise with power $Bk_{\mathrm{B}} \times T_0 \times N_{\mathrm{F}}$, where B represents the bandwidth of the signal, $k_{\mathrm{B}} = 1.381 \times 10^{-23}$, $T_0 = 290$ K, and $N_{\mathrm{F}} = 9$ dB. We implement the proposed RTI method using MATLAB R2022b [45].

Note that we do not compare the performance of the proposed binary RTI method with other RTI methods because to the best of our knowledge, there are no RTI methods with binarized SLFs. Instead, we compare two approaches for the binary RTI method, i.e., the simple and low rank approximation methods.

B. SIMULATION RESULTS

1) PERFORMANCE OF LOS/NLOS IDENTIFICATION

We first evaluate the performance of the LOS/NLOS identification method with 2D MUSIC. The number T of received signals to compute a correlation matrix $\boldsymbol{R}$ is set to $T = 30$. The LOS/NLOS identification is conducted for $N_{\mathrm{all}} = 6000$ AP-MT pairs of an AP and MT, where MTs are randomly placed within the area. Fig. 6 presents examples of the MUSIC spectrum $P_{\mathrm{MUSIC}}^{(\mathrm{dB})}(\theta, \tau) = 10 \log_{10} P_{\mathrm{MUSIC}}(\theta, \tau)$ for LOS (Fig. 6a) and NLOS (Fig. 6b) environments. In both figures, there are peaks which corresponds to AoAs and ToAs of multipath components. The red lines represents $(\hat{\theta}_{\mathrm{LOS}}(i_m, j_m), \hat{\tau}_{\mathrm{LOS}}(i_m, j_m))$. In Fig. 6a, we observe that there is a peak at the same AoA and ToA as the red line, which means that there is a peak at $(\hat{\theta}_{\mathrm{LOS}}(i_m, j_m), \hat{\tau}_{\mathrm{LOS}}(i_m, j_m))$ in the case of the LOS environment. Therefore, we can identify LOS/NLOS by comparing the spectrum at $(\hat{\theta}_{\mathrm{LOS}}(i_m, j_m), \hat{\tau}_{\mathrm{LOS}}(i_m, j_m))$ with threshold P_{th}.

Let N_{LOS} and N_{NLOS} denote the number of LOS and NLOS paths, respectively, where $N_{\mathrm{LOS}} + N_{\mathrm{NLOS}} = N_{\mathrm{all}}$, and N_{FP} and N_{FN} denote the number of NLOS paths identified as LOS paths and the number of LOS paths identified as NLOS paths, respectively. We define the false positive rate FPR and false negative rate FNR as

$$\mathrm{FPR} = \frac{N_{\mathrm{FP}}}{N_{\mathrm{NLOS}}}, \quad \mathrm{FNR} = \frac{N_{\mathrm{FN}}}{N_{\mathrm{LOS}}}.$$

Fig. 7 presents FPR and FNR vs. $P_{\mathrm{th}}^{(\mathrm{dB})} = 10 \log_{10} P_{\mathrm{th}}$. The number of antenna elements is set to $N_{\mathrm{A}} = 1, 2, 4, 8$, where $P_{\mathrm{MUSIC}}(\theta, \tau)$ with $N_{\mathrm{A}} = 1$ corresponds to the 1D MUSIC spectrum. We observe that FPR for $N_{\mathrm{A}} = 2$ is significantly improved as compared with FPR for $N_{\mathrm{A}} = 1$, which indicates that the 2D MUSIC is effective for LOS/NLOS identification.

Additionally, we also observe that FPR for $N_{\mathrm{A}} = 2, 4, 8$ are almost the same and FNR are slightly increased with N_{A}. Therefore, in the following simulation results, we set $N_{\mathrm{A}} = 2$. We evaluate the performance of the SLF estimation methods for $P_{\mathrm{th}}^{(\mathrm{dB})} = 20$ and 30. When $P_{\mathrm{th}}^{(\mathrm{dB})} = 20$, both FPR and FNR are smaller than 10^{-1}. On the other hand, when $P_{\mathrm{th}}^{(\mathrm{dB})} = 30$, FPR is smaller than 10^{-2}, but FNR is larger than 10^{-1}.

2) PERFORMANCE OF SLF ESTIMATION

We conduct the simple and low rank approximation methods by randomly selecting $M = 700$ AP-MT pairs. Fig. 8 presents SLFs estimated with the simple method. Figs. 8a and 8b correspond to the SLFs for $P_{\mathrm{th}}^{(\mathrm{dB})} = 20$ and 30, respectively. By comparing Figs. 5 and 8, we observe that the simple method can estimate the SLF. However, the estimated SLF includes impulsive noise because some pixels are not included on any measurement path. We also observe that the estimated SLF for $P_{\mathrm{th}}^{(\mathrm{dB})} = 30$ includes impulsive noise in more pixels than that for $P_{\mathrm{th}}^{(\mathrm{dB})} = 20$. The reason is that when $P_{\mathrm{th}}^{(\mathrm{dB})} = 30$, more false negative errors are included in the LOS/NLOS identification, as illustrated in Fig. 7. Specifically, many LOS paths are identified as NLOS paths.

Estimated SLFs with the low rank optimization method with $P_{\mathrm{th}}^{(\mathrm{dB})} = 20$ are presented in upper subfigures of Fig. 9, where Figs. 9a, 9b, and 9c correspond to $\boldsymbol{Z}^{(\mathrm{LR})}$, $\boldsymbol{Z}^{(\mathrm{Med})}$, and $\boldsymbol{Z}^{(\mathrm{Bin})}$, respectively. We set $\gamma = 0.1$ for the nuclear optimization. We observe that $\boldsymbol{Z}^{(\mathrm{LR})}$ is similar to the SLF in Fig. 8a, which is an estimated SLF by the simple method. However, the impulsive noise can be reduced via median filtering because the SLF is relaxed to real values. As depicted in Fig. 9b, almost all pixels with impulsive noise are discarded in $\boldsymbol{Z}^{(\mathrm{Med})}$. Fig. 10a presents the empirical probability density function (EPDF) of $\boldsymbol{Z}^{(\mathrm{Med})}$. As illustrated in the figure, EPDF is a bimodal distribution, where the lower clump corresponds to pixels without any objects and the higher clump corresponds to pixels that may include physical objects. Therefore, we can apply the Otsu's threshold selection, to binarize the pixels. Fig. 9c presents the binarized SLF $\boldsymbol{Z}^{(\mathrm{Bin})}$. We observe that the low rank approximation method can obtain a finer SLF than the simple method.

Estimated SLFs with the low rank optimization method with $P_{\mathrm{th}}^{(\mathrm{dB})} = 30$ are presented in lower subfigures of Fig. 9, where Figs. 9d, 9e, and 9f correspond to $\boldsymbol{Z}^{(\mathrm{LR})}$, $\boldsymbol{Z}^{(\mathrm{Med})}$, and $\boldsymbol{Z}^{(\mathrm{Bin})}$, respectively. Since the LOS/NLOS identification with $P_{\mathrm{th}}^{(\mathrm{dB})} = 30$ exhibits a higher false negative rate and the nuclear optimization reduces the rank of $\boldsymbol{Z}^{(\mathrm{LR})}$, $\boldsymbol{Z}^{(\mathrm{LR})}$ in Fig. 9d includes more pixels with smaller non-zeros values than in $\boldsymbol{Z}^{(\mathrm{LR})}$ in Fig. 9a. Therefore, although impulsive noise can be removed by median filtering, $\boldsymbol{Z}^{(\mathrm{Med})}$ in Fig. 9e also includes pixels with smaller values than $\boldsymbol{Z}^{(\mathrm{Med})}$ in Fig. 9b. The result affects the performance of binarization. Fig. 10b presents the EPDF of $\boldsymbol{Z}^{(\mathrm{Med})}$ for $P_{\mathrm{th}}^{(\mathrm{dB})} = 30$, which is a bimodal distribution as $\boldsymbol{Z}^{(\mathrm{Med})}$ for $P_{\mathrm{th}}^{(\mathrm{dB})} = 20$. However, because it is a more spread distribution, it is difficult to discriminate the two clumps with an adequate threshold. Therefore, as shown in Fig. 9f, most of the pixels are decided to be zero.

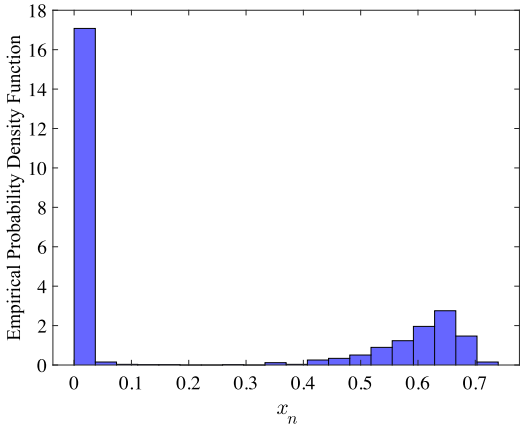

(a) $P_{\mathrm{th}}^{(\mathrm{dB})} = 20$ [dB].

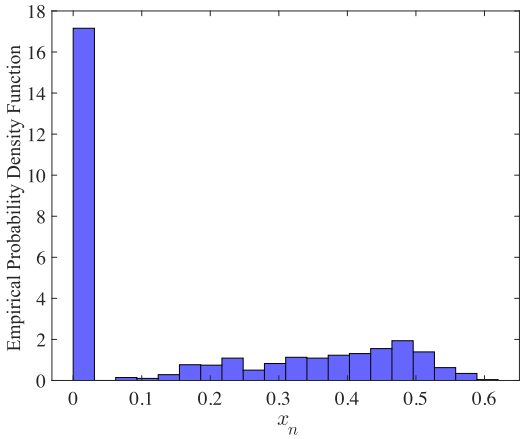

(b) $P_{\mathrm{th}}^{(\mathrm{dB})} = 30$ [dB].

FIGURE 10. Empirical probability density function of median filtered estimated spatial loss field.

VI. CONCLUSION

In this study, we have investigated SLF estimation in factory environments, where there are several metallic objects, metallic walls, and a metallic ceiling, which cause a severe multipath fading channel. To estimate the SLF in such a severe environment, we proposed the binary RTI method, where elements in a SLF are binarized. The simulation results demonstrate that the binary RTI method can estimate the SLF by combining it with the 2D MUSIC-based LOS/NLOS identification. We have evaluated the estimated SLFs for threshold parameter $P_{\mathrm{th}}^{(\mathrm{dB})} = 20$ and 30. Both FPR and FNR are smaller than 10^{-1} when $P_{\mathrm{th}}^{(\mathrm{dB})} = 20$. Meanwhile, FNR is larger than 10^{-1} when $P_{\mathrm{th}}^{(\mathrm{dB})} = 30$. From the simulation results, we have observed that the estimated SLFs with $P_{\mathrm{th}}^{(\mathrm{dB})} = 20$ are better than those with $P_{\mathrm{th}}^{(\mathrm{dB})} = 30$. The result indicates that the LOS/NLOS identification is a key component in the binary RTI method, and should be further investigated in the future research.

Since the purpose of this study is to propose the idea of the binary RTI method and evaluate its basic performance, certain unresolved issues remain in this research:

- Although we adopt the 2D MUSIC method, there have been some techniques for LOS/NLOS identification [46], [47]. The LOS/NLOS identification is a crucial and difficult research topic that should be investigated by considering these existing techniques.
- In the LOS/NLOS identification, we assumed that MTs are perfectly localized by a localization scheme, such as a LiDAR-based localization technique. However, this is not cost-effective because additional hardware for LiDAR is required. We will consider localization techniques based on radio signals for the binary RTI method.
- We have two methods to estimated SLFs: the simple greedy method and the low-rank optimization method. The former method is simple; however, it cannot completely remove impulsive noise in the estimated SLF. On the other hand, the latter method can obtain a finer SLF than the former method; however, it requires a significant computational cost especially for the nuclear optimization. To implement a more cost-effective and accurate estimator, we need to investigate other approaches.
- The estimated binarized SLF can be adopted for designing wireless networks in factory environments such as relay node placement techniques [48].
- More sophisticated network designs can be realized if 3D SLFs are obtained. To do so, the binary RTI problem should be formulated in the 3D space.

We will address these technical issues in our future research.

REFERENCES

[1] B. Singh, Z. Li, O. Tirkkonen, M. A. Uusitalo, and P. Mogensen, "Ultra-reliable communication in a factory environment for 5G wireless networks: Link level and deployment study," in *Proc. IEEE 27th Annu. Int. Symp. Pers., Indoor, Mobile Radio Commun. (PIMRC)*, Sep. 2016, pp. 1–5.

[2] G. Hampel, C. Li, and J. Li, "5G ultra-reliable low-latency communications in factory automation leveraging licensed and unlicensed bands," *IEEE Commun. Mag.*, vol. 57, no. 5, pp. 117–123, May 2019.

[3] O. Al-Saadeh, K. Hiltunen, K. Kittichokechai, A. Shapin, M. Gerami, H. Asplund, E. Wang, G. Wikstrom, and J. Sachs, "5G ultra-reliable low-latency communication for factory automation at millimetre wave bands," in *Proc. IEEE Global Commun. Conf. (GLOBECOM)*, Dec. 2019, pp. 1–6.

[4] A. M. Ramly, N. F. Abdullah, and R. Nordin, "Cross-layer design and performance analysis for ultra-reliable factory of the future based on 5G mobile networks," *IEEE Access*, vol. 9, pp. 68161–68175, 2021.

[5] E. A. Oyekanlu, A. C. Smith, W. P. Thomas, G. Mulroy, D. Hitesh, M. Ramsey, D. J. Kuhn, J. D. Mcghinnis, S. C. Buonavita, N. A. Looper, M. Ng, A. Ng'oma, W. Liu, P. G. Mcbride, M. G. Shultz, C. Cerasi, and D. Sun, "A review of recent advances in automated guided vehicle technologies: Integration challenges and research areas for 5G-based smart manufacturing applications," *IEEE Access*, vol. 8, pp. 202312–202353, 2020.

[6] M. Barring, O. Iupikov, A. A. Glazunov, M. Ivashina, J. Berglund, B. Johansson, J. Stahre, F. Harrysson, U. Engstrom, and M. Friis, "Factory radio design of a 5G network in offline mode," *IEEE Access*, vol. 9, pp. 23095–23109, 2021.

[7] S. Jiang and A. Y. C. Nee, "A novel facility layout planning and optimization methodology," *CIRP Ann.*, vol. 62, no. 1, pp. 483–486, 2013.

[8] A. Kokkas and G.-C. Vosniakos, "An augmented reality approach to factory layout design embedding operation simulation," *Int. J. Interact. Design Manuf.*, vol. 13, no. 3, pp. 1061–1071, Apr. 2019.

[9] J. Wilson and N. Patwari, "Radio tomographic imaging with wireless networks," *IEEE Trans. Mobile Comput.*, vol. 9, no. 5, pp. 621–632, May 2010.

[10] O. Kaltiokallio, M. Bocca, and N. Patwari, "Enhancing the accuracy of radio tomographic imaging using channel diversity," in *Proc. IEEE 9th Int. Conf. Mobile Adhoc Sensor Syst. (MASS)*, Oct. 2012, pp. 254–262.

[11] Z. Wang, H. Liu, B. Xiangyuan, and A. Jianping, "A chirp-FFT approach to mitigate multipath influence on radio tomographic imaging," in *Proc. Int. Conf. Wireless Commun. Signal Process.*, Oct. 2013, pp. 1–6.

[12] B. R. Hamilton, X. Ma, R. J. Baxley, and S. M. Matechik, "Propagation modeling for radio frequency tomography in wireless networks," *IEEE J. Sel. Topics Signal Process.*, vol. 8, no. 1, pp. 55–65, Feb. 2014.

[13] B. Wei, A. Varshney, N. Patwari, W. Hu, T. Voigt, and C. T. Chou, "DRTI: Directional radio tomographic imaging," in *Proc. 14th Int. Conf. Inf. Process. Sensor Netw.*, Apr. 2015, pp. 166–177.

[14] M. Takahiro, K. Yokota, K. Takemoto, S. Hara, F. Ono, K. Takizawa, and R. Miura, "Multi-dimensional wireless tomography using tensor-based compressed sensing," *Wireless Pers. Commun.*, vol. 96, no. 3, pp. 3361–3384, Oct. 2017.

[15] K. Huang, S. Tan, Y. Luo, X. Guo, and G. Wang, "Enhanced radio tomographic imaging with heterogeneous Bayesian compressive sensing," *Pervasive Mobile Comput.*, vol. 40, pp. 450–463, Sep. 2017.

[16] D. Romero, D. Lee, and G. B. Giannakis, "Blind radio tomography," *IEEE Trans. Signal Process.*, vol. 66, no. 8, pp. 2055–2069, Apr. 2018.

[17] S. Xu, H. Liu, F. Gao, and S. Chen, "Experimental verification: Enabling obstacle mapping based on radio tomographic imaging," in *Proc. IEEE 88th Veh. Technol. Conf. (VTC-Fall)*, Aug. 2018, pp. 1–5.

[18] S. Xu, H. Liu, F. Gao, and Z. Wang, "Compressive sensing based radio tomographic imaging with spatial diversity," *Sensors*, vol. 19, no. 3, p. 439, Jan. 2019.

[19] Z. Wang, X. Guo, and G. Wang, "Exploring the Laplace prior in radio tomographic imaging with sparse Bayesian learning towards the robustness to multipath fading," *Sensors*, vol. 19, no. 23, p. 5126, Nov. 2019.

[20] K. Huang and Z. Yang, "Noise adaptive optimization scheme for robust radio tomographic imaging based on sparse Bayesian learning," *IEEE Access*, vol. 8, pp. 118174–118182, 2020.

[21] Q. Guo, Y. Li, X. Liang, J. Dong, and R. Cheng, "Through-the-wall image reconstruction via reweighted total variation and prior information in radio tomographic imaging," *IEEE Access*, vol. 8, pp. 40057–40066, 2020.

[22] E. Iradier, L. Fanari, I. Bilbao, J. Montalban, P. Angueira, O. Seijo, and I. Val, "Analysis of NOMA-based retransmission schemes for factory automation applications," *IEEE Access*, vol. 9, pp. 29541–29554, 2021.

[23] R. O. Schmidt, "Multiple emitter location and signal parameter estimation," *IEEE Trans. Antennas Propag.*, vol. AP-34, no. 3, pp. 276–280, Mar. 1986.

[24] M. Kotaru, K. Joshi, D. Bharadia, and S. Katti, "SpotFi: Decimeter level localization using WiFi," in *Proc. ACM Conf. Special Interest Group Data Commun.*, Aug. 2015, pp. 269–282.

[25] X. Li, S. Li, D. Zhang, J. Xiong, Y. Wang, and H. Mei, "Dynamic-MUSIC: Accurate device-free indoor localization," in *Proc. ACM Int. Joint Conf. Pervasive Ubiquitous Comput.*, Sep. 2016, pp. 196–207.

[26] Y. Miao, E. Tanghe, J.-I. Takada, T. Pedersen, P. Laly, D. P. Gaillot, M. Lienard, L. Martens, and W. Joseph, "Measurement-based feasibility exploration on detecting and localizing multiple humans using MIMO radio channel properties," *IEEE Access*, vol. 8, pp. 3738–3750, 2020.

[27] D. I. Shuman, S. K. Narang, P. Frossard, A. Ortega, and P. Vandergheynst, "The emerging field of signal processing on graphs: Extending high-dimensional data analysis to networks and other irregular domains," *IEEE Signal Process. Mag.*, vol. 30, no. 3, pp. 83–98, May 2013.

[28] T. Matsuda, F. Ono, and S. Hara, "Graph Laplacian-based sequential smooth estimator for three-dimensional RSS map," *IEICE Trans. Commun.*, vol. 104, no. 7, pp. 738–748, 2021.

[29] N. Duffield, "Network tomography of binary network performance characteristics," *IEEE Trans. Inf. Theory*, vol. 52, no. 12, pp. 5373–5388, Dec. 2006.

[30] M. Cheraghchi, A. Karbasi, S. Mohajer, and V. Saligrama, "Graph-constrained group testing," *IEEE Trans. Inf. Theory*, vol. 58, no. 1, pp. 248–262, Jan. 2012.

[31] M. Mukamoto, T. Matsuda, S. Hara, K. Takizawa, F. Ono, and R. Miura, "Adaptive Boolean network tomography for link failure detection," in *Proc. IFIP/IEEE Int. Symp. Integr. Netw. Manage. (IM)*, May 2015, pp. 646–651.
[32] N. Bartolini, T. He, V. Arrigoni, A. Massini, F. Trombetti, and H. Khamfroush, "On fundamental bounds on failure identifiability by Boolean network tomography," *IEEE/ACM Trans. Netw.*, vol. 28, no. 2, pp. 588–601, Apr. 2020.
[33] S. Zhang, H. Wan, and X. Zhao, "A Boolean network tomography based method for deterministic multi-point fault detection," in *Proc. IEEE Global Commun. Conf. (GLOBECOM)*, Dec. 2021, pp. 1–6.
[34] R. Dorfman, "The detection of defective members of large populations," *Ann. Math. Statist.*, vol. 14, no. 4, pp. 436–440, Apr. 1943.
[35] J. G. Proakis and M. Salehi, *Digital Communications*, 5th ed. McGraw-Hill, 2008.
[36] D. Shi, H. Mi, E. G. Collins, and J. Wu, "An indoor low-cost and high-accuracy localization approach for AGVs," *IEEE Access*, vol. 8, pp. 50085–50090, 2020.
[37] H. Jo and E. Kim, "New Monte Carlo localization using deep initialization: A three-dimensional LiDAR and a camera fusion approach," *IEEE Access*, vol. 8, pp. 74485–74496, 2020.
[38] Q. Zou, Q. Sun, L. Chen, B. Nie, and Q. Li, "A comparative analysis of LiDAR SLAM-based indoor navigation for autonomous vehicles," *IEEE Trans. Intell. Transp. Syst.*, vol. 23, no. 7, pp. 6907–6921, Jul. 2022.
[39] Q. Huang and N. Lu, "Optimized real-time MUSIC algorithm with CPU-GPU architecture," *IEEE Access*, vol. 9, pp. 54067–54077, 2021.
[40] F.-G. Yan, X. Li, T. Jin, L. Liu, and M. Jin, "A real-valued polynomial rooting method for fast direction of arrival estimation with large uniform linear arrays," *IEEE Access*, vol. 7, pp. 122330–122341, 2019.
[41] X. Han, J. Wu, L. Wang, Y. Chen, L. Senhadji, and H. Shu, "Linear total variation approximate regularized nuclear norm optimization for matrix completion," *Abstract Appl. Anal.*, vol. 2014, May 2014, Art. no. 765782.
[42] A. K. Jain, *Fundamentals of Digital Image Processing*. Upper Saddle River, NJ, USA: Prentice-Hall, Jan. 1989.
[43] N. Otsu, "A threshold selection method from gray-level histograms," *IEEE Trans. Syst., Man, Cybern., Syst.*, vol. SMC-9, no. 1, pp. 62–66, Feb. 1979.
[44] *EEM-RTM*. Accessed: Sep. 12, 2022. [Online]. Available: http://www.e-em.co.jp/rtm/index.html
[45] The MathWorks, Inc. *MATLAB*. Accessed: Sep. 13, 2022. [Online]. Available: https://www.mathworks.com/
[46] C. Wu, Z. Yang, Z. Zhou, K. Qian, Y. Liu, and M. Liu, "PhaseU: Real-time LOS identification with WiFi," in *Proc. IEEE Conf. Comput. Commun.*, Apr. 2015, pp. 2038–2046.
[47] Z. Cui, Y. Gao, J. Hu, S. Tian, and J. Cheng, "LOS/NLOS identification for indoor UWB positioning based on Morlet wavelet transform and convolutional neural networks," *IEEE Commun. Lett.*, vol. 25, no. 3, pp. 879–882, Mar. 2021.
[48] H. Kapil and C. S. R. Murthy, "A pragmatic relay placement approach in 3-D space and Q-learning-based transmission scheme for reliable factory automation applications," *IEEE Syst. J.*, vol. 12, no. 1, pp. 823–833, Mar. 2018.

TAKAHIRO MATSUDA (Member, IEEE) received the B.E. (Hons.), M.E., and Ph.D. degrees in communications engineering from Osaka University, in 1996, 1997, and 1999, respectively. He joined the Department of Communications Engineering, Graduate School of Engineering, Osaka University, in 1999, where he was an Assistant Professor, from 1999 to 2005, a Lecturer, from 2005 to 2009, and an Associate Professor, from 2009 to 2018. He is currently a Professor with the Department of Computer Science, Graduate School of Systems Design, Tokyo Metropolitan University. His research interests include performance analysis and the design of communication networks and wireless communications. He is a member of IPSJ and a Senior Member of IEICE. He received the Best Tutorial Paper Award and the Best Magazine Paper Award from IEICE ComSoc, in 2012, and the Best Paper Award from IEICE, in 2014.

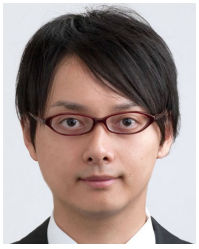

YOSHIAKI NISHIKAWA received the B.E. and M.E. degrees in communications engineering from Osaka University, in 2008 and 2010, respectively. He has been with NEC Corporation, since 2010. His research interests include mobile traffic/radio measurement, analytics, optimization, and visualization.

EIJI TAKAHASHI received the B.E. and M.E. degrees in electrical engineering and the D.Sc. degree in global information and telecommunication studies from Waseda University, in 1998, 2000, and 2003, respectively. He was a Research Associate with the Global Information and Telecommunication Institute, Waseda University, from 2000 to 2004. He was also a Visiting Industrial Fellow with the University of California at Berkeley, from 2009 to 2010. He has been with NEC Corporation, since 2004. His research interests include mobile traffic/radio measurement, analytics, optimization, and application-aware radio access network (RAN) intelligent control. He received the Telecom System Technical Premium Award from the Telecommunications Advancement Foundation, in 2006, and the Best Paper Award at IEEE CCNC, in 2017.

TAKEO ONISHI received the B.S., M.S., and D.Sc. degrees in physics from The University of Tokyo, in 2002, 2004, and 2008, respectively. He has been a Researcher with NEC Corporation, since 2008. His research interests include mobile traffic/radio measurement, analytics, optimization, and application-aware radio access network (RAN) intelligent control. He received the Best Paper Award at the Information Processing Society of Japan (IPSJ) DICOMO Symposium, in 2015, and the Best Paper Award at IEEE CCNC, in 2017.

TOSHIKI TAKEUCHI (Member, IEEE) received the B.S. degree in computer science and the M.S. degree in information sciences from Tohoku University, in 2000 and 2002, respectively. He has been with NEC Corporation, since 2002, where he has been involved in the research and development on cellular networks, software-defined radios, and radio signal analysis. His research interests include baseband signal processing and analysis, and processing architecture for communication systems. He is a member of IEICE.